CrossMark
click for updates

Synthesis and characterisation of bismacrocyclic DO3A-amide derivatives – an approach towards metal-responsive PARACEST agents†

Nevenka Cakić,[a] Tatjana Ž. Verbić,[b] Ratomir M. Jelić,[c] Carlos Platas-Iglesias[d] and Goran Angelovski*[a]

Three new bismacrocyclic Ln^{3+} chelates consisting of triamide derivatives of cyclen with glycine, methyl and *tert*-butyl substituents ($\mathbf{L^{1-3}}$, respectively) linked to an acyclic EGTA-derived calcium chelator were synthesised as potential MRI contrast agents (EGTA – ethylene glycol-bis(2-aminoethylether)-*N*,*N*,*N'*,*N'*-tetraacetic acid). Eu^{3+} and Yb^{3+} complexes of $\mathbf{L^{1-3}}$ were investigated as chemical exchange saturation transfer (CEST) agents. Moderate to minor CEST effects were observed for $\mathbf{Eu_2L^1}$, $\mathbf{Eu_2L^2}$ and $\mathbf{Yb_2L^2}$ complexes in the absence of Ca^{2+}, with negligible changes upon addition of this metal ion. Luminescence steady-state emission and lifetime experiments did not reveal any changes in the coordination environment of the complexes, while the number of inner-sphere water molecules remained constant in the absence and presence of Ca^{2+}. The protonation constants of $\mathbf{Eu_2L^1}$ and $\mathbf{Eu_2L^2}$ and stability constants of their complexes with Ca^{2+}, Mg^{2+} and Zn^{2+} were determined by means of potentiometric titrations. The results show that the charge of the complex dramatically affects the protonation constants of the EGTA-binding unit. The stability constants of the complexes formed with Ca^{2+}, Mg^{2+} and Zn^{2+} are several orders of magnitude lower than those of EGTA. These findings indicate that the nature of Ln^{3+} chelates and their charge are the main reasons for the observed results and weaker response of these EGTA-derived triamide derivatives compared to their tricarboxylate analogues.

Introduction

The continuous development of contrast agents (CAs) for magnetic resonance imaging (MRI) has provided a wide range of structurally different compounds with a range of diagnostic and therapeutic applications.[1,2] The first generation and the most widely used MRI contrast agents are based on paramagnetic Gd^{3+} complexes or superparamagnetic iron–oxide nanoparticles (T_1- and T_2-shortening agents, respectively). Although these CAs remain extensively investigated in basic research and in clinical medicine, they exhibit certain limitations related to their lack of tissue specificity and response to the chemical environment. Therefore, alternative approaches for producing image contrasts that provide additional information are greatly appreciated, leading to the development of several methodologies based on novel types of CAs.[3] Among these, the mechanism for altering MR contrast based on chemical exchange saturation transfer (CEST) has been recently established.[4] This technique has been known and used in nuclear magnetic resonance (NMR) for more than four decades, however only lately has it attracted greater attention due to its capability to generate an MRI contrast on its own, and also due to its high sensitivity towards changes in the microenvironment.[5] CEST imaging requires sufficiently slow exchange on the magnetic resonance time scale to allow selective irradiation of the protons of interest. The rate of exchange (k_{ex}) that occurs between the two magnetically distinct environments must not be greater than the difference in frequency between them ($\Delta\omega$), while several other physicochemical parameters can also affect CEST MR contrast mechanisms, including the relaxation rates of the two pools involved in chemical exchange, temperature and concentration.[6] Furthermore, a methodology that exploits particular classes of paramagnetic

[a] *MR Neuroimaging Agents, Max Planck Institute for Biological Cybernetics, Spemannstr. 41, 72076 Tübingen, Germany.*
E-mail: goran.angelovski@tuebingen.mpg.de; Fax: +49 7071 601 919;
Tel: +49 7071 601 916
[b] *Department of Analytical Chemistry, Faculty of Chemistry, University of Belgrade, Studentski trg 12-16, 11000 Belgrade, Serbia*
[c] *Faculty of Medicinal Science, University of Kragujevac, S. Markovića 69, 34000 Kragujevac, Serbia*
[d] *Centro de Investigaciones Científicas Avanzadas (CICA) and Departamento de Química Fundamental, Universidade da Coruña, Campus da Zapateira, Rúa da Fraga 10, 15008 A Coruña, Spain*
†Electronic supplementary information (ESI) available: Luminescence emission spectra, equilibrium constants and distribution diagrams. See DOI: 10.1039/c5dt04625d

lanthanide complexes for introducing tissue contrast *via* a CEST mechanism has also been developed. These complexes are specifically designed to shift exchangeable protons (–NH, –OH, –SH or bound water) further away from the bulk water allowing their distinct saturation, consequently reducing the intensity of the bulk water MR signal and hence producing the change in MRI contrast.[7]

The dependence of CEST contrast on diverse factors, including those involving paramagnetic (PARACEST) agents, can be used for the detection of specific biological processes in tissues by means of MRI. Consequently, various molecular imaging probes responsive to particular molecular events – the so called bioresponsive or "smart contrast agents" (SCAs) – have been designed.[2] In most of the cases, MRI signal changes are triggered by the variation in hydration number or rotation dynamics for the T_1- and T_2-based CA. On the other hand, signal differences produced by CEST agents are caused by the exchange rate and the chemical shift of the exchangeable proton pool, making CEST agents extremely sensitive to environmental changes, and leading to the fast development of responsive CEST agents. The most widely investigated probes of this class show response to pH and temperature, which allow a direct read-out of these relevant physiological parameters in the disease state.[8] However, systems that provide responses to metabolites, biologically relevant ions, enzyme or redox activity have also been reported.[6]

The usage of SCAs in MRI for observing specific biological processes is an extremely promising and potentially very beneficial approach to study various functional processes at the molecular and cellular level. For example, successful monitoring of Ca^{2+} would be an extremely important step for the understanding of basic physiological processes in the brain. To date, there is a single report of PARACEST agents that provide responses to this metal ion. The lanthanide ion chelator consisted of the tetraamide derivative of cyclen and four imino(diacetate) moieties that were envisaged to interact with Ca^{2+}. The corresponding Yb^{3+} and Eu^{3+} complexes were shown to provide CEST responses to Ca^{2+}; however, Mg^{2+} induced similar CEST changes.[9]

On the other hand, excellent and selective responses to Ca^{2+} were previously obtained for a series of GdDO3A-based mono- and bismacrocyclic SCAs.[10,11] In either of the cases, the organic molecule was comprised of two different moieties: a cyclen-based ring(s) appended with acetate arms for Gd^{3+} chelation and an acyclic EGTA-derived part (EGTA – ethylene glycol-bis(2-aminoethylether)-*N,N,N′,N′*-tetraacetic acid), as a high affinity and selective calcium chelator. The detailed studies on these systems revealed that Ca-induced alteration of the hydration number (q) was the major factor responsible for the longitudinal relaxivity (r_1) change.[10] The q alteration is the direct consequence of the change in coordination of the carboxylate groups in the EGTA-derived chelator in the major square antiprismatic (SAP) isomer, which flips from the Gd^{3+} coordination environment to Ca^{2+} upon its addition. Moreover, the amide groups of the EGTA-derived chelator are also
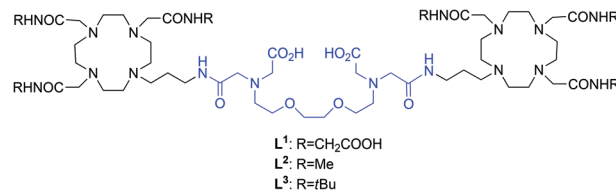

Chart 1 Chemical structures of ligands L[1–3] investigated in this work.

expected to be in the vicinity of the lanthanide ion in the presence or absence of Ca^{2+}.[11]

Having these insights on the specific coordination aspects that produce remarkable r_1 changes on Gd-based Ca-responsive SCAs, we sought to investigate their structural analogues that could potentially serve as responsive PARACEST agents. However, polyamino polycarboxylate DOTA/DO3A-type ligands are not suitable for providing a CEST effect due to the rapid exchange of the coordinated water molecule, hence they should be converted into slow-exchanging species.[1] This can be achieved by replacing the polyanionic arms of the ligand with the neutral ones, thereby decreasing the water exchange rate of the complex and making the agents suitable for PARACEST.[12,13] The most commonly investigated ligands for this purpose are tetraamide derivatives of DOTA, especially DOTAM-gly and its derivatives, although DO3A and DO2A amide derivatives have also been reported.[14] Thus, in an attempt to prepare Ca^{2+} responsive PARACEST agents we designed three different bismacrocyclic ligands, each of them bearing a standard EGTA-derived Ca-chelator coupled to amide-type macrocyclic chelators for the complexation of lanthanide metal ions. We varied the groups on the amide moieties aiming to investigate the effect of charge, hydrophobicity and steric hindrance. This resulted in the use of glycine, methyl and *tert*-butyl substituents (L[1–3], respectively) to replace the six acetic moieties of the T_1-responsive SCA (Chart 1). Upon their synthesis, various physicochemical aspects were investigated, including their CEST effect, hydration number assessment by means of time-resolved luminescence decay measurements, NMR studies and estimations of stability constants with endogenous metal ions by means of potentiometric titrations. CEST studies and luminescence lifetime measurements in the presence of Ca^{2+} were also carried out to assess the responsiveness of the synthesized agents to this metal ion.

Results and discussion

Synthesis of the ligands

The desired ligands were prepared according to a convenient six-step procedure (Scheme 1). The synthesis commenced from the commercially available cyclen, which was monoalkylated with benzyl(3-bromopropyl)carbamate **1** to give the building block **2**. The installation of different amide substituents was accomplished by alkylation of **2** with particular halogenides
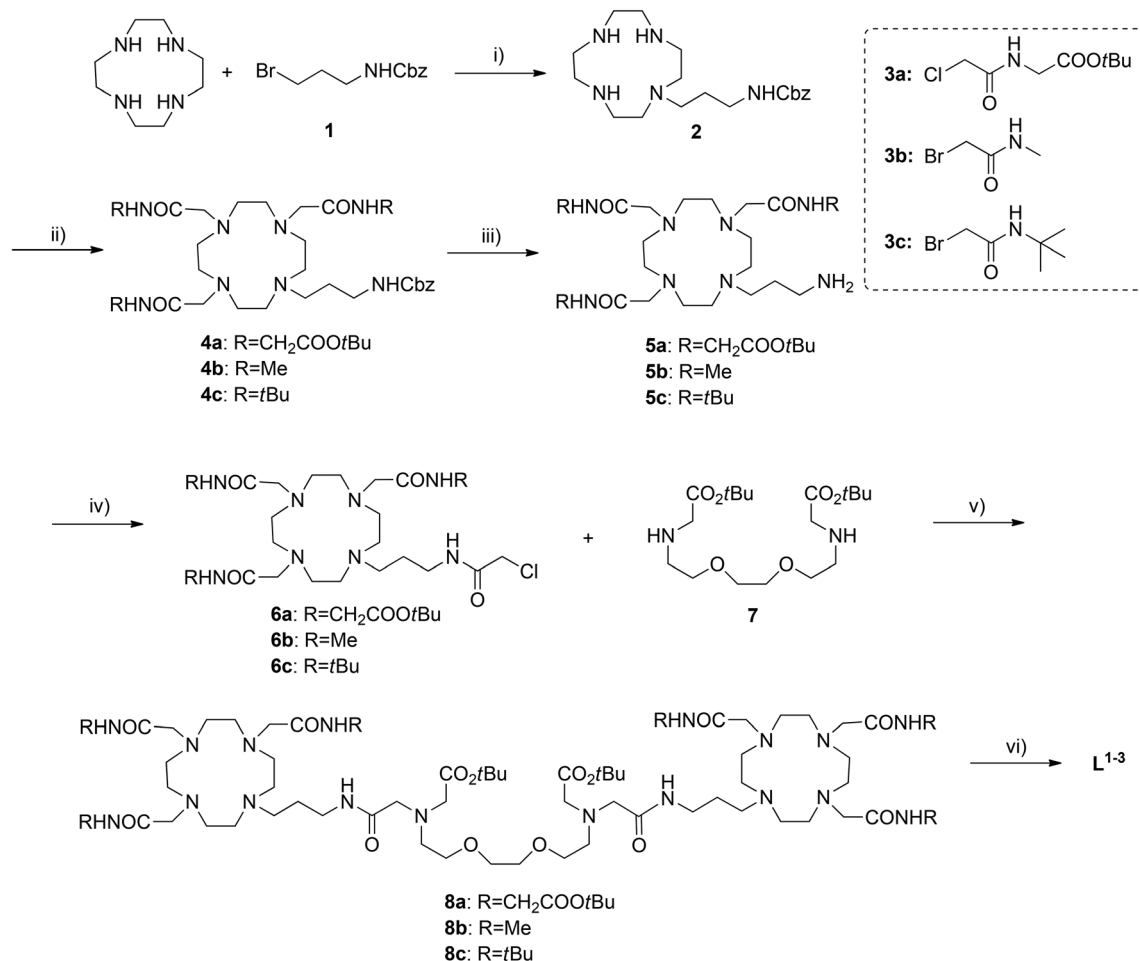
Scheme 1 Synthesis of the ligands L^{1-3}. Reagents and conditions: (i) Et$_3$N, CH$_2$Cl$_2$, RT, 59%. (ii) **3a–c**, K$_2$CO$_3$, CH$_3$CN, 70 °C, 66–83%. (iii) H$_2$, Pd/C, EtOH, RT, 92–96%. (iv) (ClCH$_2$CO)$_2$O, Et$_3$N, CH$_3$CN, RT, 74–82%. (v) K$_2$CO$_3$, KI, CH$_3$CN, 70 °C, 67–79%. (vi) HCl or HCOOH, RT, 86–93%.

3a–c in acetonitrile. The primary amines **5a–c** were obtained by reductive hydrogenation of **4a–c** in ethanol using 10% Pd on carbon as a catalyst. Further coupling of the obtained amides **6a–c** with amine **7** led to the protected bismacrocyclic ligands **8a–c**, which were treated with hydrochloric or formic acid to afford the desired ligands L^{1-3}. Finally, bimetallic Eu^{3+} or Yb^{3+} complexes were prepared by mixing the ligands with the corresponding LnCl$_3$ salt while maintaining the pH value between 6 and 7.

CEST properties

All the Z-spectra had been initially acquired at 25 °C with identical concentrations of the complexes (15 mM per Ln^{3+}). **Eu$_2$L^1** exhibited a weak CEST effect at 57 ppm, which is attributed to the proton exchange between the Eu-bound and bulk water. Temperature enhancement to 37 °C had a noticeable influence on the CEST effect resulting in an almost double increase in intensity and an upfield shift of 3 ppm (Fig. 1a and b). Previously it was shown that PARACEST agents are more suitable for noninvasive MRI thermometry methods than those depending on T_1 relaxation-time changes, chemical shift or

the diffusion coefficient of bulk water. In the former case a strong linear dependence of the chemical shift of the bound water pool with temperature was observed (~0.5 ppm °C^{-1}), while methods based on the determination of diffusion coefficients present low temperature sensitivity (~0.01 ppm °C^{-1}).[15] The CEST effect observed for **Eu$_2$L^1** is in good correlation with these findings, showing a shift of 3 ppm for the increase in temperature of 12 °C (~0.25 ppm °C^{-1}). However, the addition of Ca^{2+} (up to 10 equiv.) did not provoke a marked change in the CEST effect at any of the investigated temperatures. This result suggests that Ca^{2+} addition does not trigger important changes in the coordination environment of the paramagnetic Eu^{3+} centre, unlike the Gd-based Ca-sensitive systems containing acetate pendant arms.

The Z-spectra were also recorded using solutions of the complexes with chelators L^{2-3}, which possess a net positive charge. For the ligand with N-methylamide groups, both **Eu$_2$L^2** and **Yb$_2$L^2** complexes showed a very weak CEST effect upon saturation of the resonances corresponding to the coordinated water molecule (~5% and 1% at 53 ppm and 230 ppm, respectively). Similar to **Eu$_2$L^1**, a very small quenching of the CEST
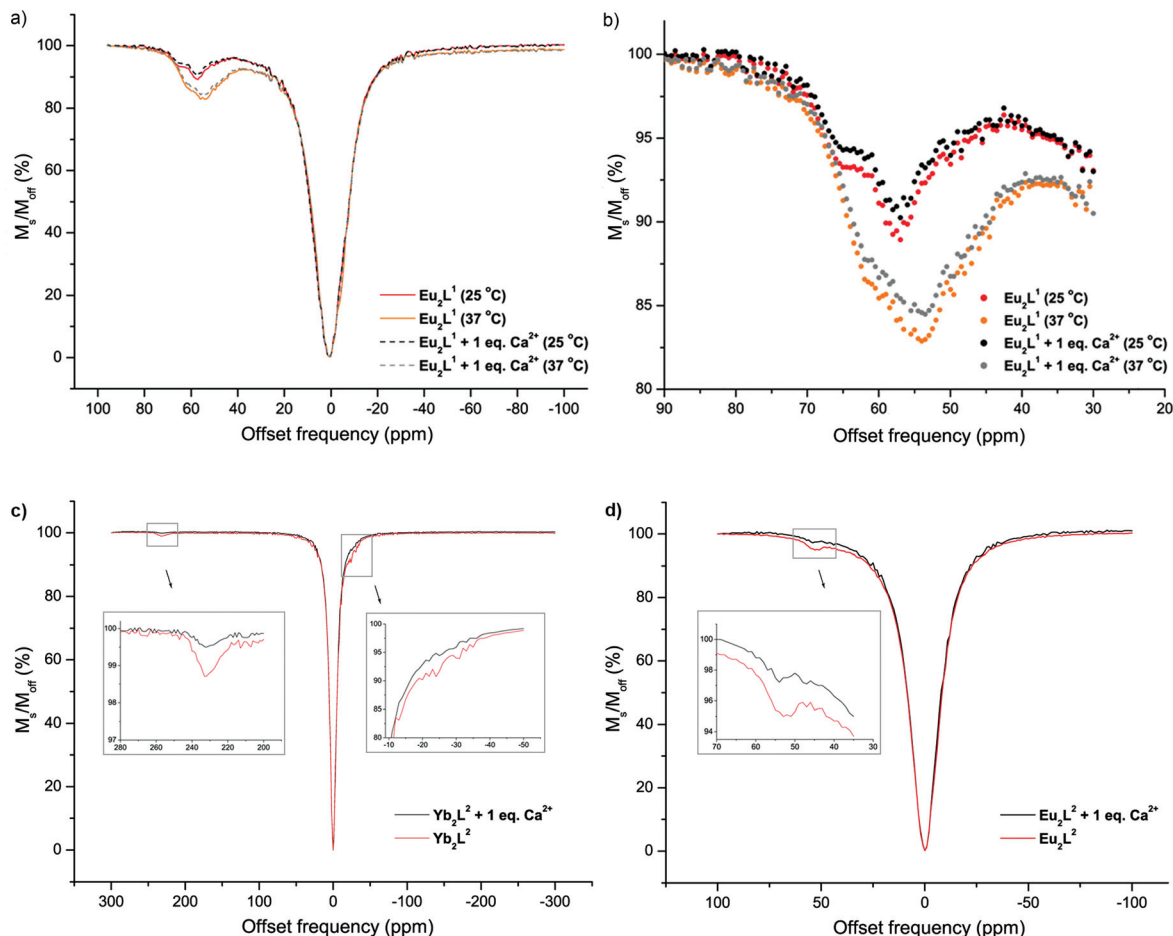
Fig. 1 The CEST spectra of 15 mM complexes (irradiation time 3 s, B_1 = 25 µT) recorded in the absence (red) and presence (black) of 1 equiv. of Ca^{2+} for: (a) Eu_2L^1, recorded at 25 and 37 °C, showing signals at 57 ppm and 54 ppm, respectively; (b) Eu_2L^1 (magnified CEST effects, conditions provided under (a); (c) Yb_2L^2, insets show magnified signals originating from bound water (230 ppm) and amide (∼−24 ppm) protons; (d) Eu_2L^2 the inset shows the magnified signal originating from bound water (53 ppm).

signal was observed upon Ca^{2+} addition in both of these complexes (Fig. 1c and d). Moreover, the Yb_2L^2 complex provides a weak CEST effect at an offset frequency of ∼−24 ppm that remains nearly unaffected upon addition of Ca^{2+}. This CEST effect is attributed to exchangeable NH protons, and is in agreement with previous findings that revealed CEST peaks due to amide protons in Yb^{3+} complexes in the range −15 to −29 ppm.[16–18] Finally, the Z-spectra of the complexes with bulky *tert*-butyl substituents Eu_2L^3 and Yb_2L^3 did not show any CEST effect in the presence or absence of Ca^{2+} (data not shown).

Apparently, the acquired Z-spectra and obtained CEST properties indicated that the prepared DO3A-amide Eu^{3+} and Yb^{3+} complexes likely have different coordination characteristics from their carboxylic Gd^{3+} analogues. The strongest CEST signal was obtained for the DO3AM-gly-type derivative (Eu_2L^1), suggesting that the polarity of the side arms and the overall charge of the complexes play important roles in determining the exchange rate of the coordinated water molecule responsible for the CEST signal. Previous reports showed that the

introduction of bulky groups into the amide side arms of DOTAM derivatives accelerates water exchange in a favourable way for the CEST effect,[19] although the opposite effects were also obtained.[20] In this study the CEST effect gradually decreases on the DO3AM-type bismacrocyclic derivatives towards the less polar and bulky substituents resulting in the preferred order CH_2COOH > CH_3 > $C(CH_3)_3$. However, the absence of any response to Ca^{2+} (its addition did not cause observable reductions or increases in CEST effects on $Eu_2L^{1–2}$ or Yb_2L^2) suggested that the coordination environment of the paramagnetic ions in these triamide systems has been changed compared to their tricarboxylic analogues, requiring further investigation.

Luminescence experiments

The hydration states in the presence and absence of Ca^{2+} can provide a good indication of potential changes in the environment of the paramagnetic ion upon Ca^{2+} addition. Thus, the luminescence emission lifetimes of $Eu_2L^{1–3}$ were recorded in H_2O and D_2O, and the hydration numbers (q) were calculated

Table 1 Calculated q values for the Eu_2L^{1-3} with and without addition of Ca^{2+}

| Complex	Without Ca^{2+}			+Ca^{2+} (1 equiv.)		
	k_{H_2O} (ms^{-1})	k_{D_2O} (ms^{-1})	q	k_{H_2O} (ms^{-1})	k_{D_2O} (ms^{-1})	q
Eu_2L^1	1.58	0.66	1.08	1.56	0.66	1.05
Eu_2L^2	2.16	0.71	1.71	2.17	0.73	1.70
Eu_2L^3	1.76	0.75	1.18	1.76	0.79	1.13

according to a previously established methodology (Table 1).[21] The obtained results show that the q number stays constant, within the experimental error, upon calcium addition to all the three investigated complexes. This behaviour is opposite that of DO3A-based analogue SCA systems, which showed an increase in the number of inner-sphere water molecules upon Ca^{2+} addition.[10,11] Further, the findings indicate that Eu_2L^1 and Eu_2L^3 are monohydrated complexes, while the less sterically hindered complex Eu_2L^2 displays an equilibrium between dihydrated and monohydrated species. The absence of prominent CEST effects upon Ca^{2+} addition to aqueous solutions of Eu_2L^{1-3} can certainly be correlated with hydration states remaining constant, indicating that the addition of Ca^{2+} does not provoke significant changes in the coordination environment of the lanthanide ion.

The luminescence steady-state emission spectra of Eu_2L^{1-3} in H_2O were also recorded. Similarly to the decay experiments, addition of Ca^{2+} did not produce any significant change in the intensity or shape of the major $^5D_0 \rightarrow {}^7F_{0-4}$ transitions (Fig. S1 in the ESI†). However, further splitting of the signals due to the $^5D_0 \rightarrow {}^7F_1$ and $^5D_0 \rightarrow {}^7F_4$ transitions and change in the intensity ratios of $^5D_0 \rightarrow {}^7F_1$ and $^5D_0 \rightarrow {}^7F_2$ transitions at 590 and 615 nm were observed at basic pH for Eu_2L^{1-2}, suggesting the change in polarisability of the axial donor and the local symmetry at the metal centre (Fig. S2 in the ESI†). The major cause for these spectral alterations was apparently a change in protonation states of amines from the EGTA-derived chelator and inner-sphere water molecules (see below).

NMR studies

The ^1H NMR spectra of Eu_2L^{1-3} complexes were recorded in D_2O solutions at pD ~ 8.0 (Fig. 2). They present relatively broad resonances that spread over the range ~−20 to 30 ppm due to the paramagnetic shifts induced by the metal ion. The spectrum of Eu_2L^1 points to the presence of at least three different isomers in solution. It is well-known that DOTA-like complexes may exist in solution as two different isomers providing either a square-antiprismatic (SAP) or a twisted-square antiprismatic (TSAP) coordination around the lanthanide(III) ion. These isomers differ either in the orientation of the pendant arms of the macrocycle, which is often denoted as Δ or Λ, or the conformation of the cyclen moiety [(δδδδ) or (λλλλ)].[22,23] In Eu^{3+} complexes of DOTA and DO3A derivatives the signals of the pseudo-axial protons on the cyclen rings are usually found between 24 and 45 ppm in the square antipris-
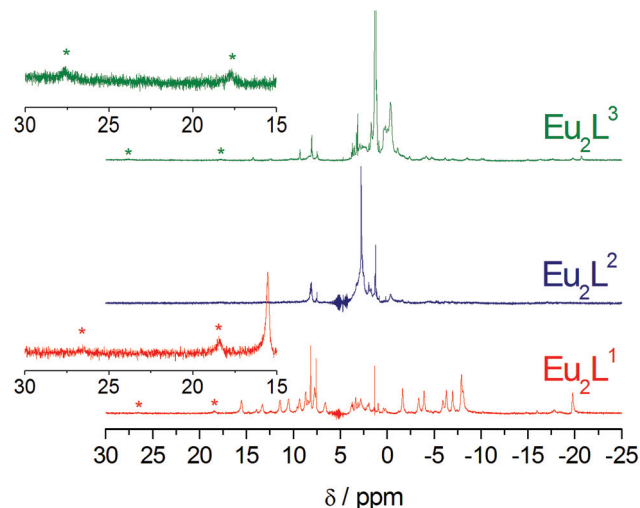
Fig. 2 ^1H NMR spectra of Eu_2L^{1-3} recorded in D_2O solutions (pD ~ 8.0, 25 °C). The asterisks indicate the most shifted resonances of axial protons of the macrocycle in the SAP form. The insets show enhancements of the 15–30 ppm regions obtained for Eu_2L^1 and Eu_2L^3.

matic (SAP) isomer and below 25 ppm in the twisted-square antiprismatic (TSAP) isomer.[24–29] In the case of Eu_2L^1, one of the species present in solution shows signals in the range +15 to −20 ppm, while the second isomer with a smaller population display signals due to the macrocyclic axial protons at lower fields, one clearly visible at ~19 and a broader one at 27 ppm. These results point to the presence of two nine coordinate species with SAP and TSAP coordination around the metal ion, the overall population being dominated by the TSAP form (ca. 90%). This ratio of species is completely inverse to that found for the responsive Gd-DO3A complexes where only the SAP isomer changes its hydration upon binding with Ca^{2+}.[11] Moreover, a third set of signals dominated by two resonances at ca. 7.5–8.5 ppm is also observed. The spectrum of Eu_2L^2 is dominated by the latter signals, which on the basis of the hydration number of this complex can be assigned to a complex DO3A-type species containing two coordinated water molecules. Similarly to Eu_2L^1, the spectrum of Eu_2L^3 displays signals due to the monohydrated SAP and TSAP isomers, again with the minor SAP isomer representing ca. 30% of the population of the TSAP isomer. Additionally, the species attributed to the bis-hydrated complex are also present, which is likely the reason why luminescence lifetime measurements provide hydration numbers slightly higher than one (Table 1).

Potentiometric titrations

To further characterize Eu_2L^{1-2} complexes, their protonation constants, as well as stability constants of the complexes formed with Ca^{2+}, Mg^{2+} and Zn^{2+} were determined by means of potentiometric titrations (Fig. S3 and S4 in the ESI†).

Complex formation of Eu–H–L$^{1-2}$ systems. Binary complexes formed in the studied aqueous solutions ($t = 25 \pm 1$ °C, $I = 0.1$ M NaCl, pH range 4–10) were characterised using the general equilibrium relation shown in eqn (1) (charges were

**Table 2** Experimentally determined protonation constants of Eu_2L^{1-2} complexes[a] compared to EDTA, EGTA and EGTA–bisamide protonation constants reported in the literature

	Eu_2L^1	Eu_2L^2	EDTA[b]	EGTA[b]	EGTA– bisamide[b]
$\log K_1^{\mathrm{H}}$	8.72	7.34	10.17	9.47	6.79
$\log K_2^{\mathrm{H}}$	8.29	5.20	6.11	8.85	5.87
$\log K_3^{\mathrm{H}}$	6.82	4.43	2.68	2.26	2.79
$\log K_4^{\mathrm{H}}$	—	—	2.00	2.00	
$[Eu_2(OH)_2L] + 2H^+ \rightleftarrows$ $[Eu_2L(H_2O)_2]$	9.56	9.09			

[a] I = 0.1 M (NaCl), t = 25 ± 1 °C. [b] I = 0.1 M (KCl), ref. 35.

Fig. 3 Distribution diagram of Eu^{3+}–L^1 species at [L] : [Eu] = 1 : 2 concentration ratio; total Eu^{3+} concentration 0.5 mM; I = 0.1 M (NaCl), t = 25 ± 1 °C.

omitted for simplicity), and the corresponding cumulative stability constants provided in eqn (2).

$$pEu + qH + rL \rightleftarrows Eu_pH_qL_r; \ \beta_{p,q,r} \ (L = L^1 \text{ or } L^2) \quad (1)$$
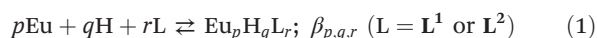
$$\beta_{p,q,r} = \frac{[Eu_pH_qL_r]}{[Eu]^p[H]^q[L]^r} \quad (2)$$

In order to study speciation in the three-component systems Eu–H–L or Eu–OH–L (L = L^1 or L^2), it was necessary to characterize the binary equilibria, *i.e.*, hydrolysis of Eu^{3+} and the ligands' proteolytic equilibria. The equilibrium constants of Eu^{3+} hydrolysis were taken from the literature,[30] and the ligand protonation constants calculated using the ADMET Predictor software[31] (Table S1 in the ESI†), showing good agreement with previously published values for DOTAM-type systems.[32] The equilibrium constants of the complexes were determined using the Hyperquad 2008 software (using ionic product value pK_w = 13.77).[33] Species distribution diagrams were plotted according to calculated constants using the HySS software.[34]

The equilibrium constants of Eu–H–L complexes were determined by acid–base potentiometric titrations (Tables 2 and S2 in the ESI†). Analysis of the potentiometric titration data was performed to find the model that gives the best fit to the experimental data (statistical parameters which determine the quality of fit are provided in Table S2 in the ESI†). The calculations revealed the formation of $[Eu_2(H_nL)]$ (n = 1, 2, 3) as well as $[Eu_2(L)]$ complexes. The formation of $[Eu_2L(OH)_2]$ complexes was also noticed. The obtained protonation constants were compared to those previously published for ethylenediaminetetraacetic acid (EDTA), EGTA and EGTA–bisamide (Table 2),[35] while the experimentally determined stability constants with standard deviations are provided in the ESI (Table S2†).

The first two protonation constants ($\log K_1^{\mathrm{H}}$ and $\log K_2^{\mathrm{H}}$) stand for protonation of the amine nitrogen atoms of the EGTA-derived part. These values are quite different for Eu_2L^1 and Eu_2L^2. The complex Eu_2L^1 displays a higher basicity similar to EDTA and especially EGTA; this can be explained by the overall charge as the presence of six carboxylate groups on the macrocycles in Eu_2L^1 neutralize the positive charge of two bound Eu^{3+} ions. This can also be the reason for the relatively
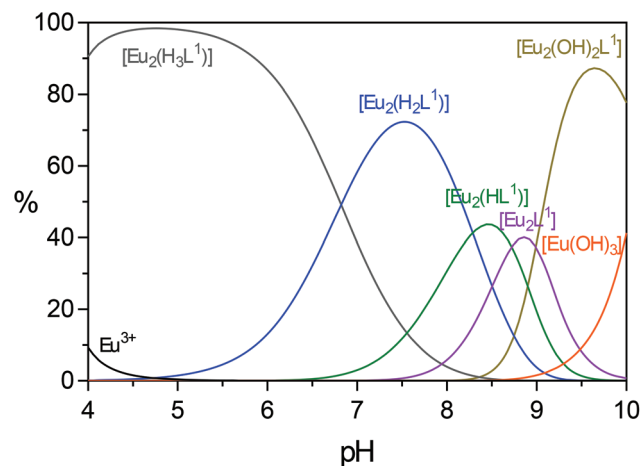
high $\log K_3^{\mathrm{H}}$. On the other hand, the highly positively charged Eu_2L^2 behaves similar to the EGTA–bisamide, having one neutral and one acidic amine nitrogen, respectively, and a lower $\log K_3^{\mathrm{H}}$ value compared with Eu_2L^1. Distribution diagrams of species in the Eu_2L^{1-2} system, for the concentration ratio [L] : [Eu] = 1 : 2, indicate this different behaviour (Fig. 3 and S5 in the ESI†). The dominating complex species at pH < 5 is $[Eu_2(H_3L)]$, a complex in which Eu^{3+} ions are coordinated to the ligand L^1 or L^2 and the EGTA part is triprotonated. Consequently, the species $[Eu_2(H_3L^1)]$ and $[Eu_2(H_3L^2)]$ have a maximum concentration at pH 4.7 and 4.2, respectively. As pH values increase, the $[Eu_2(H_3L)]$ complex releases protons forming $[Eu_2(H_2L)]$, $[Eu_2(HL)]$, and $[Eu_2(L)]$, and finally the $[Eu_2L(OH)_2]$ complex. The complex $[Eu_2(L^1)]$ starts to form at pH 7 and reaches the maximal concentration at pH 8.9 (Fig. 3), while the complex $[Eu_2(L^2)]$ starts to form at pH 5 and reaches the maximal concentration at pH 8.7 (Fig. S5 in the ESI†). Moreover, the hydroxo complex $[Eu_2L(OH)_2]$ in both cases starts to form around pH 8, and reaches the maximum concentration around pH 9.5. The hydroxide $Eu(OH)_3$ begins to form around pH 8.5, and its concentration increases with the further increase of pH.

Complex formation of $[Eu_2L]$ with Ca^{2+}, Mg^{2+} or Zn^{2+}; heteronuclear systems. The stability constants for the complex formation between Eu_2L^{1-2} and M (M = Ca^{2+}, Mg^{2+} or Zn^{2+}) are represented using the general equilibrium relation shown in eqn (3) (charges were omitted for simplicity), while the corresponding cumulative stability constant is given by eqn (4).

$$pEu + qH + rL + mM \rightleftarrows Eu_pH_qL_rM_m; \ \beta_{p,q,r,m} \quad (3)$$

$$\beta_{p,q,r,m} = \frac{[Eu_pH_qL_rM_m]}{[Eu]^p[H]^q[L]^r[M]^m} \quad (4)$$

These stability constants were also determined by acid–base potentiometric titrations. The obtained values were compared with those previously reported for EDTA, 2,2′-oxybis-(ethyl-

Table 3 Experimentally determined stability constants of Eu^{3+}–L–M (L = L^1 or L^2; M = Ca^{2+}, Mg^{2+} or Zn^{2+}) complexes[a] compared to Eu^{3+}–L–M (L = EDTA, OBETA or EGTA; M = Ca^{2+}, Mg^{2+} or Zn^{2+}) stability constants reported in the literature

	L^1	L^2	EDTA[b]	OBETA[c]	EGTA[b]
Ca^{2+}	4.60	4.24	10.61	9.77	10.86
Mg^{2+}	4.08	3.38	8.69	7.95	5.28
Zn^{2+}	6.93	5.59	16.50	15.00	12.60
	$\log K_{Eu_2CaL}/\log K_{Eu_2MgL}$			$\log K_{CaL}/\log K_{MgL}$	
	1.13	1.25	1.22	1.23	2.06
	$\log K_{Eu_2ZnL}/\log K_{Eu_2CaL}$			$\log K_{ZnL}/\log K_{CaL}$	
	1.51	1.32	1.56	1.54	1.16

[a] I = 0.1 M (NaCl), t = 25 ± 1 °C. [b] I = 0.1 M (KCl for EDTA, KNO_3 for EGTA), ref. 36 and 37. [c] I = 0.1 M (KNO_3), ref. 38.
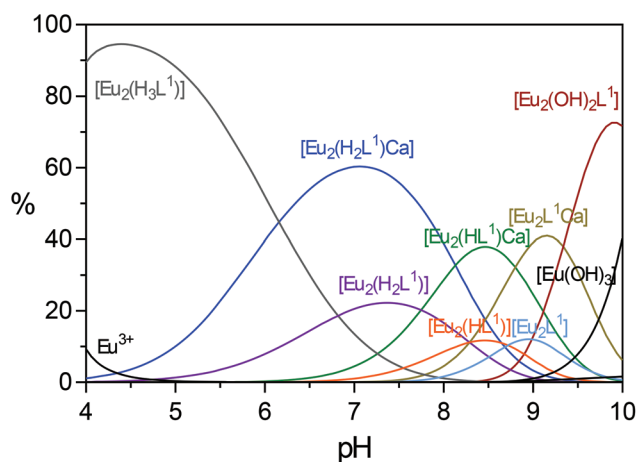
Fig. 4 Distribution diagram of Eu^{3+}–L^1–Ca species at [Eu] : [L^1] : [Ca] concentration ratio = 2 : 1 : 1; total Eu^{3+} concentration 0.5 mM; I = 0.1 M (NaCl), t = 25 ± 1 °C.

amine)-N,N,N',N'-tetraacetic acid (OBETA) and EGTA (Table 3),[36–38] while the final set of complexes existing in the studied aqueous solutions and experimentally determined stability constants with standard deviations and statistical parameters showing the quality of fit are provided in the ESI (Table S3†). Finally, the corresponding distribution diagrams of the species in the Eu^{3+}–L–M systems (L = L^1 or L^2 and M = Ca^{2+}, Mg^{2+} or Zn^{2+}) for the concentration ratio [Eu] : [L] : [M] = 2 : 1 : 1 are also plotted (Fig. 4 and S6–10 in the ESI†).

The stability constants obtained for $Eu_2L^{1,2}$ with the investigated metal ions were several orders of magnitude lower than that for the well-studied EDTA, OBETA or EGTA chelators with the same metals. There might be a few reasons for such behaviour. First, the binding affinity of bisamide–bisacid chelators ($Eu_2L^{1,2}$) is expected to be weaker than in the case of tetraacid chelators (EDTA, OBETA or EGTA) due to the reduction in the number of negatively charged carboxylate chelating groups. Next, the additional positive charge on the macrocyclic ring (especially valid for Eu_2L^2) induces the repulsion between the $Eu_2L^{1,2}$ complex and the positively charged metal complex.

This phenomenon can also be confirmed by the differences in stability constants between Eu_2L^1 and Eu_2L^2, where the former exhibits slightly higher values for all three metal ions due to its lower net positive charge when compared to the latter complex. Finally, the reduced flexibility of the EGTA-derived chelator in $Eu_2L^{1,2}$ due to the presence of bulky appended macrocycles may prevent efficient wrapping around the metal ion compared with the case of flexible EDTA, OBETA or EGTA chelators.

Furthermore, the obtained stability constants also indicate a decrease in the selectivity of $Eu_2L^{1,2}$ for Ca^{2+}, Mg^{2+} and Zn^{2+}. This phenomenon can be easily followed by comparing the ratio of stability constants for a single chelator with two different metals (Table 3). As it can be seen, the ratio of $\log K_{Eu_2CaL}/\log K_{Eu_2MgL}$ or $\log K_{Eu_2ZnL}/\log K_{Eu_2CaL}$ for both $Eu_2L^{1,2}$ is comparable to analogous ratios obtained for EDTA and OBETA despite much lower $\log K_{ML}$ values for $Eu_2L^{1,2}$ and the structural similarity of the chelating site to EGTA. This loss of selectivity of $Eu_2L^{1,2}$ for Ca^{2+} vs. Mg^{2+} could be explained by the same reasons that lead to the drop in $\log K_{Eu_2ML}$ values. Namely, the reduced flexibility of $Eu_2L^{1,2}$ compared to EGTA prevents better recognition and size match of the EGTA-derived chelator with Ca^{2+} than with Mg^{2+}, while the increase in the positive charge of $Eu_2L^{1,2}$ additionally impairs binding to metal ions and their recognition.

Despite the considerably lower stability constant values for the three investigated metals, the distribution diagrams indicate that heteronuclear complexes are the major species at the physiological pH (Fig. 4 and S6–10 in the ESI†). The heteronuclear complexes $[Eu_2(H_nL^1)Ca]$ (n = 0, 1 or 2) are probably formed by the following reaction:

$$[Eu_2(H_nL^1)] + Ca^{2+} \rightleftarrows [Eu_2(H_nL^1)Ca]; \quad n = 0, 1 \text{ or } 2.$$

Consequently, the dominating complex at lower pH values is $[Eu_2(H_3L^1)]$, with a maximal concentration at pH around 4.5 (Fig. 4). Similar assumptions can be made according to the obtained distribution diagrams of other heteronuclear complexes, $[Eu_2(H_nL^1)Mg]$ and $[Eu_2(H_nL^1)Zn]$ (Fig. S6 and S7 in the ESI†). The protonated heteronuclear complex, $[Eu_2(H_2L^1)Ca]$ has a maximum concentration at pH around 7 and is fairly stable (Table S3 in the ESI†). The formation of the complex $[Eu_2(HL^1)Ca]$ starts at around pH 6 and reaches the maximum concentration at pH 8.2. The complex $[Eu_2(L^1)Ca]$ starts to form at pH 7 and reaches the maximum concentration around pH 9.

Conclusions

In this work we synthesised three different bismacrocyclic DO3A-amide derivatives appended with the EGTA-derived chelator. The amides had glycine, methyl and tert-butyl as substituents resulting in ligands $L^{1–3}$, respectively. The paramagnetic complexes of $L^{1–3}$ were prepared and various aspects of their physicochemical behaviour were investigated. Eu_2L^1 exhibited a greater CEST effect than Eu_2L^2 and Yb_2L^2

complexes, while $\mathbf{Eu_2L^3}$ and $\mathbf{Yb_2L^3}$ showed the absence of any CEST effect, suggesting that the polarity of substituents and the overall charge of the complexes play an essential role in the existence of the CEST effect. Addition of Ca^{2+} led to negligible changes in the CEST effects in the investigated complexes. The luminescence steady-state emission and lifetime measurements confirmed the insensitivity of $\mathbf{Eu_2L^{1-3}}$ towards Ca^{2+} as the inner-sphere hydration of the complexes remained intact in the presence and absence of Ca^{2+}. These findings were in line with the results from ^{1}H NMR experiments which indicated the presence of different mono- or bis-hydrated isomers of $\mathbf{Eu_2L^{1-3}}$ in solution. However, the analysis of NMR data revealed a switch of the SAP/TSAP isomer population for DO3A-amide complexes when compared to the previously investigated responsive Gd-DO3A complexes. In DO3A-amides, the TSAP isomer appeared to be the major species, which does not change the coordination environment around the Ln^{3+} ion (*i.e.* inner-sphere hydration) upon complexation with Ca^{2+}. It has been shown that the population of the TSAP isomer increases upon increasing the steric hindrance for the coordination of the pendant arms to the lanthanide(III) ion.[39] Thus, it is likely that the presence of the amide substituents in $\mathbf{Eu_2L^{1-3}}$ introduces some steric hindrance that favors the TSAP isomer over the SAP one. Finally, the results from potentiometric titrations showed a great dependence of protonation constants on the net charge of the complexes $\mathbf{Eu_2L^{1-2}}$. They bind Ca^{2+} with reduced affinity and with a lower selectivity towards Mg^{2+} or Zn^{2+} compared to the original EGTA chelator, which is a consequence of their positive charge and reduced flexibility of the binding site.

The results presented here suggest that replacement of carboxylate for amide groups in macrocycles changes the coordination to lanthanide metal ions and results in alterations in their behaviour. Consequently, the interaction with metal ions such as Ca^{2+} is dramatically affected, converting the Ca-sensitive DO3A-derived bioresponsive T_1 agent into non-sensitive DO3A-amide-derived potential CEST agents. Obviously, further adjustments in the microenvironment around the paramagnetic metal are required to obtain efficient CEST agents, prior or post interactions with the desired metal ion. Thus, the present work provides an important set of information that will aid better design of future bioresponsive agents for CEST MRI.

Experimental section

General remarks

Commercially available reagents and solvents were used without further purification. Compounds $\mathbf{1}$,[40] $\mathbf{3a}$,[17] $\mathbf{3b}$,[41] $\mathbf{3c}$[19] and $\mathbf{7}$[10] were synthesised according to previously published procedures. Purification of the synthesised compounds was performed using silica gel 60 (0.03–0.2 mm) from Carl Roth (Germany). Standard 0.1 M HCl and NaOH solutions were prepared from ampoules (Titrisol, Merck, Darmstadt, Germany) and potentiometrically standardised. Standard 5 mM Ca^{2+},

Mg^{2+}, and Zn^{2+} solutions were prepared from appropriate salts and standardised by titration with an EDTA solution. Acros Organics buffers were used for electrode calibration (phthalate pH 4.00, phosphate pH 7.00, and carbonate pH 10.00). All NMR spectra were acquired on a Bruker Avance III 300 MHz, processed using TopSpin 2.1 (Bruker GmbH), and analysed with TopSpin 2.1 or ACD/SpecManager 9.0 (Advanced Chemistry Development, Inc.). The concentration of the complexes was determined using the bulk magnetic susceptibility shift (BMS).[42] ESI-HRMS were performed on a Bruker BioApex II ESI-FT-ICR, equipped with an Agilent ESI-Source, measured *via* flow injection analysis. ESI-LRMS were performed on an ion trap SL 1100 system (Agilent, Germany). Luminescence lifetime measurements were performed by using a Quanta-MasterTM 3-PH fluorescence spectrometer from Photon Technology International, Inc., (Monmouth Junction, NJ, USA). Potentiometric titrations were performed by using a Metrohm Basic Titrino 794 (Herisau, Switzerland) equipped with an InLab Micro electrode (Mettler-Toledo International Inc., Columbus, Ohio, USA).

Synthetic procedures. Benzyl(3-(1,4,7,10-tetraazacyclododecan-1-yl)propyl)carbamate (2)

Compound **2** was synthesised according to the previously described procedure for monoalkylation of cyclen,[43] using **1** as the alkylating agent.

Compound **2**: isolated yield: 59%. ^{1}H NMR (CDCl$_3$, 300 MHz), δ (ppm): 7.38–7.27 (m, 5H), 5.06 (s, 2H), 3.24–3.18 (br, 2H), 2.73–2.67 (br, 4H), 2.65–2.59 (br, 4H), 2.54–2.40 (br, 10H), 1.72–1.63 (m, 2H). ^{13}C NMR (CDCl$_3$, 75 MHz), δ (ppm): 156.6, 136.9, 128.3, 128.0, 127.8, 66.2, 52.1, 51.5, 47.0, 46.0, 45.1, 39.3, 27.5. ESI-HRMS: for $C_{19}H_{33}N_5O_2^+$: calc. 364.2707 $[M + H]^+$, found 364.2711.

General procedure for the synthesis of 4a–4c

3a, **3b** or **3c** (3.2 equiv.) was added in an already prepared suspension of **2** (1.0 equiv.) and K_2CO_3 (4.0 equiv.) in anhydrous acetonitrile. The reaction mixture was stirred at 65 °C for 18 h. After cooling, the product mixture was filtered and the solvent was removed under reduced pressure. The residue was dissolved in dichloromethane and washed twice with water. The organic layer was dried over Na_2SO_4 and then evaporated under reduced pressure to give crude **4a**, **4b** or **4c**. The compounds were purified by column chromatography over silica (eluent MeOH in CH_2Cl_2) to give **4a–c** as amorphous solids.

Compound 4a. Starting from **3a** (4.30 g, 20.7 mmol), 4.05 g of **4** (66%) was obtained. The eluent for column chromatography purification was 7% MeOH in CH_2Cl_2. ^{1}H NMR (CDCl$_3$, 300 MHz), δ (ppm): 7.28–7.22 (m, 5H), 5.00 (s, 2H), 3.84–3.73 (br, 6H), 3.29–2.36 (br, 26H), 1.62–1.52 (m, 2H), 1.37–1.31 (overlapping s, 27H). ^{13}C NMR (CDCl$_3$, 75 MHz), δ (ppm): 172.2, 171.4, 169.1, 168.9, 168.8, 156.5, 136.9, 128.4, 128.1, 127.9, 81.8, 81.3, 66.2, 57.1, 56.8, 54.1, 53.5, 52.9, 51.1, 49.9, 41.9, 41.7, 38.9, 28.1, 27.9. ESI-HRMS: for $C_{43}H_{72}N_8O_{11}^+$: calc. 899.5213 $[M + Na]^+$, found 899.5219.

Compound 4b. Starting from **3b** (5.00 g, 32.9 mmol), 4.40 g of **4b** (74%) was obtained. The eluent for column chromatography purification was 30% MeOH in CH_2Cl_2. ^1H NMR (CDCl$_3$, 300 MHz), δ (ppm): 7.38–7.27 (m, 5H), 5.08 (s, 2H), 3.23–3.17 (m, 2H), 3.03 and 3.02 (overlapping s, 6H), 2.79–2.49 (br, 27H), 1.74–1.64 (m, 2H). ^{13}C NMR (CDCl$_3$, 75 MHz), δ (ppm): 171.6, 171.3, 156.5, 136.5, 128.5, 128.2, 66.6, 59.1, 58.5, 54.0, 53.4 (br), 53.3 (br), 52.8, 39.6, 25.9, 25.8. ESI-HRMS: for $C_{28}H_{48}N_8O_5^+$: calc. 577.3820 $[M + H]^+$, found 577.3830.

Compound 4c. Starting from **3c** (4.80 g, 24.7 mmol), 4.50 g of **4c** (83%) was obtained. The eluent for column chromatography purification was 10% MeOH in CH_2Cl_2. ^1H NMR (CDCl$_3$, 300 MHz), δ (ppm): 7.28–7.25 (m, 5H), 5.0 (s, 2H), 3.52–2.65 (br, 26H), 1.85–1.61 (m, 2H), 1.29–1.27 (overlapping s, 27H). ^{13}C NMR (CDCl$_3$, 75 MHz), δ (ppm): 168.6 (br), 168.0, 155.8, 135.7, 127.5, 127.0, 65.5, 56.8 (br), 52.5, 50.6 (br), 48.7 (br), 37.7, 27.7, 27.5 (br). ESI-LRMS: for $C_{37}H_{66}N_8O_5^+$: calc. 703.5 $[M + H]^+$, found 703.5.

General procedure for the synthesis of 5a–5c

10% Pd/C was added to a solution of **4a** (3.00 g, 3.4 mmol), **4b** (3.70 g, 6.4 mmol) or **4c** (3.10 g, 4.4 mmol) in ethanol (50 mL). The resulting mixture was stirred at room temperature under a hydrogen atmosphere (3 bar) for 18 hours. The reaction was then filtered over Celite® to remove the catalyst and the solvent was removed by rotary evaporation. The residue was dissolved in CH_2Cl_2 (50 mL) and the precipitate was removed by filtration. The organic layer was dried over Na_2SO_4 and then evaporated to give **5a** (2.40 g, 94%), **5b** (2.60 g, 92%) or **5c** (2.40 g, 96%).

Compound 5a. ^1H NMR (CDCl$_3$, 300 MHz), δ (ppm): 3.77 and 3.76 (overlapping s, 6H), 3.55–2.43 (br, 26H), 1.60–1.47 (m, 2H), 1.39–1.32 (overlapping s, 27H). ^{13}C NMR (CDCl$_3$, 75 MHz), δ (ppm): 173.1, 169.2, 168.5, 81.7, 81.5, 81.3, 58.4, 57.4 (br), 50.8 (br), 48.7, 42.1 (br), 41.9 (br), 40.0 (br), 28.1 (br), 28.0 (br). ESI-HRMS: for $C_{35}H_{66}N_8O_9^+$: calc. 743.5025 $[M + H]^+$, found 743.5030.

Compound 5b. ^1H NMR (CD$_3$OD, 300 MHz), δ (ppm): 3.38–3.05 (br, 8H), 2.79–2.45 (br, 27H), 1.85–1.70 (m, 2H). ^{13}C NMR (CD$_3$OD, 75 MHz), δ (ppm): 174.2, 173.4, 170.3, 59.8, 58.9, 52.2 (br), 51.9, 51.7, 40.4, 26.3 (br), 24.9. ESI-HRMS: for $C_{20}H_{42}N_8O_3^+$: calc. 443.3453 $[M + H]^+$, found 443.3458.

Compound 5c. ^1H NMR (CDCl$_3$, 300 MHz), δ (ppm): 3.61–2.40 (br, 26H), 1.94–1.55 (m, 2H), 1.38–1.34 (overlapping s, 27H). ^{13}C NMR (CDCl$_3$, 75 MHz), δ (ppm): 171.2, 170.8, 169.9, 169.7, 66.4 (br), 58.0, 51.8, 51.7 (br), 51.6 (br), 51.5 (br), 50.7 (br), 28.8 (br), 28.5 (br). ESI-HRMS: for $C_{29}H_{60}N_8O_3^+$: calc. 569.4861 $[M + H]^+$, found 569.4866.

General procedure for the synthesis of 6a–6c

5a, **5b** or **5c** (1 equiv.) and Et$_3$N (1.5 equiv.) were dissolved in anhydrous acetonitrile. The solution was cooled to 0 °C under a nitrogen atmosphere and a solution of chloroacetic anhydride (1.3 equiv.) in acetonitrile was added dropwise. The reaction was stirred at 0 °C for an additional 3 h. The solvent was evaporated from the reaction mixture and the crude product was purified by column chromatography over silica gel (eluent MeOH in CH_2Cl_2) to give **6a**, **6b** or **6c**.

Compound 6a. Starting from **5a** (2.10 g, 2.8 mmol), 1.89 g of **6a** (82%) was obtained. The eluent for column chromatography purification was 10% MeOH in CH_2Cl_2. ^1H NMR (CDCl$_3$, 300 MHz), δ (ppm): 4.00 (s, 2H), 3.82 (s br, 4H), 3.74 (s br, 2H), 3.34–2.22 (br, 26H), 1.68–1.58 (m, 2H), 1.38–1.32 (overlapping s, 27H). ^{13}C NMR (CDCl$_3$, 75 MHz), δ (ppm): 172.1, 168.9, 168.7, 166.4, 81.7, 81.4, 57.6, 56.9, 50.8 (br), 42.7, 41.7, 38.1, 29.6, 28.0, 24.6. ESI-HRMS: for $C_{37}H_{67}ClN_8O_{10}^+$: calc. 841.4561 $[M + Na]^+$, found 841.4562.

Compound 6b. Starting from **5b** (2.30 g, 5.2 mmol), 2.20 g of **6b** (82%) was obtained. The eluent for column chromatography purification was 30% MeOH in CH_2Cl_2. ^1H NMR (CD$_3$OD, 300 MHz), δ (ppm): 4.16 (s br, 2H), 3.80–3.20 (br, 22H), 3.08–2.98 (br, 4H), 2.84 and 2.82 (overlapping s, 9H), 2.09–2.01 (m, 2H). ^{13}C NMR (CD$_3$OD, 75 MHz), δ (ppm): 173.4 (br), 169.6, 166.2 (br), 57.6, 55.9, 53.7, 52.9 (br), 51.3 (br), 50.9 (br), 50.5, 43.5, 37.9, 37.1 (br), 36.2 (br), 26.8, 26.6, 23.8 (br). ESI-HRMS: for $C_{22}H_{43}ClN_8O_4^+$: calc. 541.2988 $[M + Na]^+$, found 541.2995.

Compound 6c. Starting from **5c** (2.10 g, 3.7 mmol), 1.76 g of **6c** (74%) was obtained. The eluent for column chromatography purification was 30% MeOH in CH_2Cl_2. ^1H NMR (CDCl$_3$, 300 MHz), δ (ppm): 4.04 (s, 2H), 3.44–2.30 (br, 26H), 1.82–1.68 (m, 2H), 1.36–1.30 (overlapping s, 27H). ^{13}C NMR (CDCl$_3$, 75 MHz), δ (ppm): 171.8, 169.0, 52.1 (br), 51.7, 45.6, 43.9, 28.7 (br), 28.1 (br). ESI-LRMS: for $C_{31}H_{61}ClN_8O_4^+$: calc. 667.4 $[M + Na]^+$, found 667.5.

General procedure for the synthesis of 8a–8c

The reaction flask was charged with **6a**, **6b** or **6c** (1 equiv.), **7** (0.4 equiv.), K_2CO_3 (1.7 equiv.), KI (1 equiv.) and anhydrous acetonitrile and the reaction mixture was heated at 70 °C overnight under a nitrogen atmosphere. The inorganic salts were removed by filtration and the solvent was evaporated to dryness. The crude product was purified by column chromatography over silica gel using 8% MeOH in CH_2Cl_2 as the eluent to give **8a**, **8b** or **8c**.

Compound 8a. Starting from **6a** (1.30 g, 1.6 mmol), 0.90 g of **8a** (70%) was obtained. ^1H NMR (CDCl$_3$, 300 MHz), δ (ppm): 8.44 (s br, 3H), 7.93 (s br, 2H), 7.55 (s br, 3H), 3.76 and 3.75 (overlapping s, 12H), 3.69–3.53 (br, 12H), 3.43 (s, 4H), 3.33–3.20 (br, 14H), 2.91–2.30 (br, 42H), 1.58–1.55 (m, 4H), 1.38–1.34 (overlapping s, 72H). ^{13}C NMR (CDCl$_3$, 75 MHz), δ (ppm): 172.6, 171.1 (br), 169.9, 168.9, 168.4, 82.4, 81.9, 81.6, 69.6, 68.4, 58.7 (br), 57.7 (br), 51.1 (br), 50.9 (br), 50.6, 50.3, 48.5, 41.8 (br), 41.7 (br), 39.9 (br), 29.6 (br), 27.9 (br), 23.8 (br).

Compound 8b. Starting from **6b** (1.50 g, 2.9 mmol), 1.09 g of **8b** (67%) was obtained. ^1H NMR (CD$_3$OD, 300 MHz), δ (ppm): 3.89–2.4 (br, 90H), 2.14–2.04 (m, 2H), 1.84–1.74 (m, 2H), 1.55–1.52 (overlapping s, 18H). ^{13}C NMR (CD$_3$OD, 75 MHz), δ (ppm): 175.1 (br), 174.5 (br), 174.0 (br), 173.5, 173.0, 168.8, 84.8, 82.9, 71.3, 71.1, 70.2, 67.9, 60.0, 58.6 (br), 58.1 (br), 56.0, 28.6, 28.5, 26.7, 26.5.

Compound 8c. Starting from **6c** (1.20 g, 1.9 mmol), 0.98 g of **8c** (79%) was obtained. ^{1}H NMR (CDCl$_3$, 300 MHz), δ (ppm): 3.85–2.30 (br, 72H), 1.90–1.80 (m, 4H), 1.51–1.26 (overlapping s, 72H). ^{13}C NMR (CDCl$_3$, 75 MHz), δ (ppm): 169.4, 166.5, 162.8, 80.8, 67.0, 53.4, 50.1 (br), 48.6, 48.2 (br), 46.9, 44.5, 26.9 (br), 26.7 (br), 26.6 (br), 26.1 (br).

General procedure for the synthesis of L$^{1–3}$

Bismacrocycle **8a**, **8b** or **8c** was dissolved in formic acid (3 mL) and the solution was heated at 60 °C for 18 h (for potentiometric titrations, **L$^{1–2}$** were prepared by mixing **8a,b** with 4 N HCl (3 mL) in dioxane at RT for 4 hours). After the solution was cooled, formic acid was removed on the rotary evaporator. The residue was dissolved in a minimal amount of water, added dropwise to cooled acetone (−20 °C) and stored in the freezer overnight. The acetone was decanted from the solid material and the crude products **L$^{1–3}$** were obtained by drying in a vacuum.

Ligand L^1. Starting from **8a** (0.70 g, 0.4 mmol), 0.48 g of **L^1** (89%) was obtained. ^{1}H NMR (D$_2$O, 300 MHz), δ (ppm): 4.08 (s br, 4H), 3.89–3.72 (br, 16H), 3.69 (s, 2H), 3.63–3.59 (br, 6H), 3.50–2.98 (br, 56H), 2.14–2.04 (m, 4H). ^{13}C NMR (D$_2$O, 75 MHz), δ (ppm): 175.62, 175.20, 172.11 (br), 171.03, 69.62, 65.51, 55.49, 55.17, 51.64 (br), 51.30, 49.03 (br), 46.75, 42.82, 36.59, 30.30, 21.37.

Ligand L^2. Starting from **8b** (0.45 g, 0.3 mmol), 0.38 g of **L^2** (93%) was obtained. ^{1}H NMR (CD$_3$OD, 300 MHz), δ (ppm): 3.74–3.20 (br, 52H), 3.03–2.69 (br, 38H), 2.00–1.90 (m, 4H). ^{13}C NMR (CD$_3$OD, 75 MHz), δ (ppm): 173.58, 171.00, 167.59, 71.33 (br), 71.19, 68.44, 67.32, 59.39, 59.13 (br), 57.99 (br), 56.48 (br), 54.47 (br), 53.26, 52.67 (br), 50.51 (br), 37.82 (br), 26.76, 26.50, 24.25 (br).

Ligand L^3. Starting from **8c** (0.66 g, 0.4 mmol), 0.53 g of **L^3** (86%) was obtained. ^{1}H NMR (CD$_3$OD, 300 MHz), δ (ppm): 3.95–2.61 (br, 72H), 1.92–1.80 (m, 4H), 1.26–1.13 (overlapping s, 54H). ^{13}C NMR (CD$_3$OD, 75 MHz), δ (ppm): 171.10, 168.00, 166.41, 71.32, 67.16, 62.64, 55.77, 53.04 (br), 52.28 (br), 50.44 (br), 29.26 (br), 29.21 (br), 29.08.

General procedure for the preparation of Ln^{3+} complexes

The Ln^{3+} complexes of **L^2** and **L^3** were prepared by mixing the respective ligand and the LnCl$_3$ solutions in a 2 : 1 (Ln^{3+} : L) molar ratio. The exact amount of ligand was determined by elemental analysis. The solution was stirred at RT for 48 h. The pH value was adjusted to 7.0–7.5 using 1 M NaOH. The absence of a free ion (Yb^{3+} or Eu^{3+}) was verified by colorimetric assay using xylenol orange.

In the case of negatively charged **L^1**, EuCl$_3$ was added in slight excess (>2 equiv.). The mixture was stirred for 48 h at RT maintaining the pH at 7.0–7.5, using 1 M NaOH. The resulting solution was treated with Chelex 100 to remove the excess Eu^{3+} and the absence of free Eu^{3+} was verified by colorimetric assay using xylenol orange.

Luminescence lifetime experiments

The lifetime measurements were performed on a Quanta-MasterTM 3 PH fluorescence spectrometer from Photon Technology International, Inc. The measurements were performed in H$_2$O and D$_2$O (25 °C) at 5 mM Eu^{3+} concentration. The Eu^{3+} ion was directly excited at 395 nm, and the emission intensity at 615 nm was measured with a 10 μs resolution. The excitation and emission slits were set to 15 and 5 nm bandpass, respectively. Data sets are an average of 25 scans, and each reported value is the mean of three independent measurements. The obtained curves are fitted to a first-order exponential decay with $r^2 = 0.99$. The q values were calculated using eqn (5).[21]

$$q_{Eu} = 1.2 \times [k_{H_2O} - k_{D_2O} - 0.25 + 0.075 n_{O=CHN}], n = 3 \quad (5)$$

Potentiometric titrations

Experiments were performed at $t = 25 \pm 1$ °C, with a constant argon flow, using a 794 Basic Titrino automatic titrator (Metrohm, Herisau, Switzerland) equipped with an InLab Micro electrode (Mettler-Toledo International Inc., Columbus, Ohio, USA). The electrode–pH-meter system was calibrated by means of a strong acid–strong base titration in 0.1 M NaCl, using GLEE – GLass Electrode Evaluation software;[44] standard potential ($E^0 = 383.6 \pm 0.2$ mV) and slope (57.4 ± 0.1 mV) are obtained as mean values of four titrations. Hyperquad 2008 software was used to calculate protonation and stability constant values as the mean values of four titrations.[33]

Eu$_2$L (L = L^1 or L^2) protonation constant determination. Eu$_2$L complexes were previously synthesized in a solution. The concentration of stock Eu$_2$L solutions was determined according to the BMS method.[42] Stock Eu$_2$L solutions were diluted with 0.1 M NaCl to prepare working solutions ([**Eu$_2$L^1**] = 2.4547 × 10^{-4} M, [**Eu$_2$L^2**] = 4.9971 × 10^{-4} M). Prior to titration, standard HCl solution (0.0984 M; 35.0 μL for **Eu$_2$L^1**, and 60.0 μL for **Eu$_2$L^2**) was added to 4.00 mL of Eu$_2$L working solutions to reach pH 4. All probes were titrated with 2.0 μL increments of standard NaOH solution (0.1008 M) in the 4.0–10.0 pH range.

Eu$_2$L (L = L^1 or L^2) stability constants with Ca^{2+}, Mg^{2+} and Zn^{2+} determination. Prior to titration, standard HCl solution (0.0984 M; 35.0 μL for **Eu$_2$L^1**, and 60.0 μL for **Eu$_2$L^2**) and 1.0–1.1, 1.2–1.3, and 1.5–1.6 mol-equivalents of standard Ca^{2+}, Mg^{2+}, or Zn^{2+} solutions were added to 4.00 mL of Eu$_2$L working solutions and stirred for 10 minutes. All probes were then titrated with 2.0 μL increments of standard NaOH solution (0.1008 M) in the 4.0–10.0 pH range. Total concentrations of the ligand and metal ion used in each experiment are provided in the ESI.†

Notes and references

1 M. M. J. Modo and J. W. M. Bulte, *Molecular and cellular MR imaging*, CRC Press, Taylor & Francis Group, Boca Raton, London, New York, 2007.

2 A. E. Merbach, L. Helm and É. Tóth, *The chemistry of contrast agents in medical magnetic resonance imaging*, Wiley, Chichester, 2013.

3 E. Terreno, D. D. Castelli, A. Viale and S. Aime, *Chem. Rev.*, 2010, **110**, 3019–3042.

4 A. D. Sherry and M. Woods, *Annu. Rev. Biomed. Eng.*, 2008, **10**, 391–411.

5 P. C. M. van Zijl and N. N. Yadav, *Magn. Reson. Med.*, 2011, **65**, 927–948.

6 D. V. Hingorani, A. S. Bernstein and M. D. Pagel, *Contrast Media Mol. Imaging*, 2015, **10**, 245–265.

7 M. Woods, E. W. C. Donald and A. D. Sherry, *Chem. Soc. Rev.*, 2006, **35**, 500–511.

8 D. Delli Castelli, E. Terreno and S. Aime, *Angew. Chem., Int. Ed.*, 2011, **50**, 1798–1800.

9 G. Angelovski, T. Chauvin, R. Pohmann, N. K. Logothetis and É. Tóth, *Bioorg. Med. Chem.*, 2011, **19**, 1097–1105.

10 G. Angelovski, P. Fouskova, I. Mamedov, S. Canals, E. Toth and N. K. Logothetis, *ChemBioChem*, 2008, **9**, 1729–1734.

11 P. Kadjane, C. Platas-Iglesias, P. Boehm-Sturm, V. Truffault, G. E. Hagberg, M. Hoehn, N. K. Logothetis and G. Angelovski, *Chem. – Eur. J.*, 2014, **20**, 7351–7362.

12 M. Woods, D. E. Woessner, P. Y. Zhao, A. Pasha, M. Y. Yang, C. H. Huang, O. Vasalitiy, J. R. Morrow and A. D. Sherry, *J. Am. Chem. Soc.*, 2006, **128**, 10155–10162.

13 J. R. Slack and M. Woods, *J. Biol. Inorg. Chem.*, 2014, **19**, 173–189.

14 S. Viswanathan, Z. Kovacs, K. N. Green, S. J. Ratnakar and A. D. Sherry, *Chem. Rev.*, 2010, **110**, 2960–3018.

15 N. McVicar, A. X. Li, M. Suchy, R. H. E. Hudson, R. S. Menon and R. Bartha, *Magn. Reson. Med.*, 2013, **70**, 1016–1025.

16 S. Aime, D. Delli Castelli, F. Fedeli and E. Terreno, *J. Am. Chem. Soc.*, 2002, **124**, 9364–9365.

17 M. M. Ali, M. Woods, E. H. Suh, Z. Kovacs, G. Tircso, P. Y. Zhao, V. D. Kodibagkar and A. D. Sherry, *J. Biol. Inorg. Chem.*, 2007, **12**, 855–865.

18 S. Aime, A. Barge, D. D. Castelli, F. Fedeli, A. Mortillaro, F. U. Nielsen and E. Terreno, *Magn. Reson. Med.*, 2002, **47**, 639–648.

19 T. Mani, G. Tircso, O. Togao, P. Zhao, T. C. Soesbe, M. Takahashi and A. D. Sherry, *Contrast Media Mol. Imaging*, 2009, **4**, 183–191.

20 S. Aime, A. Barge, A. S. Batsanov, M. Botta, D. Delli Castelli, F. Fedeli, A. Mortillaro, D. Parker and H. Puschmann, *Chem. Commun.*, 2002, 1120–1121.

21 A. Beeby, I. M. Clarkson, R. S. Dickins, S. Faulkner, D. Parker, L. Royle, A. S. de Sousa, J. A. G. Williams and M. Woods, *J. Chem. Soc., Perkin Trans. 2*, 1999, 493–503.

22 S. Aime, M. Botta, M. Fasano, M. P. M. Marques, C. F. G. C. Geraldes, D. Pubanz and A. E. Merbach, *Inorg. Chem.*, 1997, **36**, 2059–2068.

23 D. Parker, R. S. Dickins, H. Puschmann, C. Crossland and J. A. K. Howard, *Chem. Rev.*, 2002, **102**, 1977–2010.

24 C. Adair, M. Woods, P. Y. Zhao, A. Pasha, P. M. Winters, G. M. Lanza, P. Athey, A. D. Sherry and G. E. Kiefer, *Contrast Media Mol. Imaging*, 2007, **2**, 55–58.

25 M. Regueiro-Figueroa, K. Djanashvili, D. Esteban-Gomez, T. Chauvin, E. Toth, A. de Blas, T. Rodriguez-Blas and C. Platas-Igleslas, *Inorg. Chem.*, 2010, **49**, 4212–4223.

26 M. Polasek, J. Kotek, P. Hermann, I. Cisarova, K. Binnemans and I. Lukes, *Inorg. Chem.*, 2009, **48**, 466–475.

27 F. A. Dunand, R. S. Dickins, D. Parker and A. E. Merbach, *Chem. – Eur. J.*, 2001, **7**, 5160–5167.

28 S. Aime, M. Botta and G. Ermondi, *Inorg. Chem.*, 1992, **31**, 4291–4299.

29 P. Caravan, J. J. Ellison, T. J. McMurry and R. B. Lauffer, *Chem. Rev.*, 1999, **99**, 2293–2352.

30 W. Hummel, U. Berner, E. Curti, F. J. Pearson and T. Thoenen, *Radiochim. Acta*, 2002, **90**, 805–813.

31 ADMET Predictor, Simulations Plus, Inc., Lancaster, CA, USA, ver. 7.2, 2015.

32 A. Pasha, G. Tircso, E. T. Benyo, E. Brucher and A. D. Sherry, *Eur. J. Inorg. Chem.*, 2007, 4340–4349.

33 P. Gans, A. Sabatini and A. Vacca, *Talanta*, 1996, **43**, 1739–1753.

34 L. Alderighi, P. Gans, A. Ienco, D. Peters, A. Sabatini and A. Vacca, *Coord. Chem. Rev.*, 1999, **184**, 311–318.

35 S. Aime, A. Barge, M. Botta, L. Frullano, U. Merlo and K. I. Hardcastle, *J. Chem. Soc., Dalton Trans.*, 2000, 3435–3440.

36 L. Tei, Z. Baranyai, M. Botta, L. Piscopo, S. Aime and G. B. Giovenzana, *Org. Biomol. Chem.*, 2008, **6**, 2361–2368.

37 C. De Stefano, A. Gianguzza, D. Milea, A. Pettignano and S. Sammartano, *J. Alloys Compd.*, 2006, **424**, 93–104.

38 R. Negri, Z. Baranyai, L. Tei, G. B. Giovenzana, C. Platas-Iglesias, A. C. Benyei, J. Bodnar, A. Vagner and M. Botta, *Inorg. Chem.*, 2014, **53**, 12499–12511.

39 M. Purgel, Z. Baranyai, A. de Blas, T. Rodriguez-Blas, I. Banyai, C. Platas-Iglesias and I. Toth, *Inorg. Chem.*, 2010, **49**, 4370–4382.

40 K. Dhingra, P. Fouskova, G. Angelovski, M. E. Maier, N. K. Logothetis and E. Toth, *J. Biol. Inorg. Chem.*, 2008, **13**, 35–46.

41 O. Vasalatiy, P. Y. Zhao, M. Woods, A. Marconescu, A. Castillo-Muzquiz, P. Thorpe, G. E. Kiefer and A. D. Sherry, *Bioorg. Med. Chem.*, 2011, **19**, 1106–1114.

42 D. M. Corsi, C. Platas-Iglesias, H. van Bekkum and J. A. Peters, *Magn. Reson. Chem.*, 2001, **39**, 723–726.

43 J. Massue, S. E. Plush, C. S. Bonnet, D. A. Moore and T. Gunnlaugsson, *Tetrahedron Lett.*, 2007, **48**, 8052–8055.

44 P. Gans and B. O'Sullivan, *Talanta*, 2000, **51**, 33–37.